Assessing the summer water budget of a moulin basin in the Sermeq Avannarleq ablation region, Greenland ice sheet

Daniel McGRATH,[1] William COLGAN,[1] Konrad STEFFEN,[1] Phillip LAUFFENBURGER,[2] James BALOG[3]

[1]*Cooperative Institute for Research in Environmental Sciences, University of Colorado at Boulder, Boulder, Colorado 80309-0216, USA*
E-mail: daniel.mcgrath@colorado.edu
[2]*Aerospace Engineering Sciences Department, University of Colorado at Boulder, Boulder, Colorado, 80309-0429, USA*
[3]*Extreme Ice Survey, 1435 Yarmouth Avenue, Boulder, Colorado 80304-4338, USA*

ABSTRACT. We provide an assessment of the supraglacial water budget of a moulin basin on the western margin of the Greenland ice sheet for 15 days in August 2009. Meltwater production, the dominant input term to the $1.14 \pm 0.06\,km^2$ basin, was determined from in situ ablation measurements. The dominant water-output terms from the basin, accounting for 52% and 48% of output, respectively, were moulin discharge and drainage into crevasses. Moulin discharge exhibits large diurnal variability ($0.017–0.54\,m^3\,s^{-1}$) with a distinct late-afternoon peak at 16:45 local time. This lags peak meltwater production by $\sim 2.8 \pm 4.2$ hours. An Extreme Ice Survey time-lapse photography sequence complements the observations of moulin discharge. We infer, from in situ observations of moulin geometry, previously published borehole water heights and estimates of the temporal lag between meltwater production and observed local ice surface uplift ('jacking'), that the transfer of surface meltwater to the englacial water table via moulins is nearly instantaneous (<30 min). We employ a simple crevasse mass-balance model to demonstrate that crevasse drainage could significantly dampen the surface meltwater fluctuations reaching the englacial system in comparison to moulin discharge. Thus, unlike crevasses, moulins propagate meltwater pulses to the englacial system that are capable of overwhelming subglacial transmission capacity, resulting in enhanced basal sliding.

1. INTRODUCTION

The Greenland ice sheet (GrIS) is currently losing 200–250 $Gt\,a^{-1}$ of ice through a combination of an increasingly negative surface mass balance and enhanced ice discharge from major outlet glaciers (Hanna and others, 2008; Thomas and others, 2009; Van den Broeke and others, 2009). Both in situ GPS and interferometric synthetic aperture radar (InSAR) satellite observations in the western ablation zone of the GrIS demonstrate a distinct annual ice velocity cycle, in which peak velocities are observed during the summer melt season (Zwally and others, 2002; Joughin and others, 2008; Bartholomew and others, 2010; Colgan and others, 2011). On daily and seasonal timescales, higher surface velocities have been attributed to enhanced basal sliding, which occurs when meltwater input exceeds the transmission capacity of the subglacial hydrologic network (Iken and others, 1983; Anderson and others, 2004; Shepherd and others, 2009; Bartholomew and others, 2010).

1.1. Glacier hydrology

Strong diurnal and seasonal variations in meltwater production imply that the englacial and subglacial hydrologic networks are seldom in steady state, but rather constantly adjusting to changing input volumes (Hock and Hooke, 1993; Cutler, 1998; Bartholomaus and others, 2008). At the beginning of the melt season, meltwater is delivered to a quiescent subglacial hydrologic network, which has largely closed during the winter through creep closure (Nye, 1953). As a result of initial meltwater input exceeding subglacial transmission capacity, subglacial water pressure increases, driving water into a distributed cavity network beneath the glacier, resulting in surface uplift interpreted as bed separation. This process reduces basal friction and increases basal sliding velocities (Iken and others, 1983; Willis and others, 1996; Anderson and others, 2004; Bartholomaus and others, 2008). Similar to alpine glaciers, enhanced basal sliding in the GrIS has been shown to continue as long as meltwater production exceeds subglacial transmission capacity, creating conditions of positive net water storage in the subglacial environment (Colgan and others, 2011). During the melt season, conduits enlarge by melting from the frictional heating of the flowing water, which allows the subglacial hydrologic system to evolve to accommodate larger meltwater fluxes later in the melt season (Röthlisberger, 1972; Hock and Hooke, 1993). As a result, a transition occurs mid-melt season as the subglacial transmission capacity exceeds meltwater input, and water is efficiently drained via low-pressure channels (Cutler, 1998; Bartholomew and others, 2010). Overlaid on this seasonal meltwater pattern is a diurnal meltwater input cycle, resulting in a daily cycle in which input exceeds transmission capacity (Schoof, 2010). This cycle drives localized uplift and enhanced basal sliding in the GrIS several hours after peak surface meltwater production in the late afternoon (Shepherd and others, 2009). This is followed by a surface lowering and subsequent decrease in ice velocity, presumably as the meltwater input volume falls below the efficiency of the subglacial hydrologic network (Shepherd and others, 2009).

The cumulative effect of enhanced diurnal and seasonal velocities is an increase in total annual ice displacement, the magnitude of which is positively correlated with modeled meltwater production (Zwally and others, 2002). The seasonal acceleration is most significant (~50% increase above

https://doi.org/10.3189/002214311798043735 Published online by Cambridge University Press

mean annual ice velocity) in land-terminating regions of the ice sheet, and less significant (~10–15% increase) in outlet glaciers, where velocity is more directly related to changes in back-stress at the tidewater terminus (Howat and others, 2005; Joughin and others, 2008). Observations show that ice velocities in the ablation zone respond quickly to short-term changes in meltwater production, although significant uncertainty exists in predicting how the GrIS hydrology system evolves over decadal and longer timescales to changing volumes of meltwater. One study finds no long-term (decadal) increase in mean annual ice velocity despite significant seasonal melt-driven accelerations occurring during a 17 year period (Van de Wal and others, 2008). The apparently conflicting nature of these observations highlights the uncertainty in this aspect of ice-sheet evolution and certainly warrants long-term observations in order to develop a unifying explanation.

The supraglacial hydrologic cycle is most pronounced along the marginal zone of the GrIS where the relatively high surface slope (2–5°), complex surface topography and relatively high ablation rates differ substantially from the vast interior accumulation zone. Melting of snow and glacier ice in the ablation zone produces water that flows across the ice surface, developing supraglacial streams, which can drain into surface depressions to form supraglacial lakes or drain directly into moulins (Box and Ski, 2007). Meltwater can also drain into crevasses or smaller fractures, where it may seasonally refreeze (Catania and others, 2008). Supraglacial streams evolve from interconnected runnels into an arborescent network on the ice surface, incising through thermal erosion at a rate that exceeds the surface ablation rate (Knighton, 1981; Marston, 1983). On account of the latent energy contained in liquid water, even modest water temperatures (0.005–0.01 °C) can result in channel incision rates of 3.8–5.8 cm d^{-1} (Pinchak, 1972; Marston, 1983).

Meltwater lakes are a common feature of the GrIS ablation zone. They typically range in size from a few hundred meters to >2 km in diameter, with mean water depths of 2–5 m (Box and Ski, 2007). The presence of meltwater on the ice surface, and the subsequent increase in water depth as melt lakes develop, reduces surface albedo, and increases shortwave radiation absorption, amplifying melt rates (Perovich and others, 2002). Further, meltwater lakes are observed to frequently drain over short timescales (hours to days) at discharge rates exceeding 300 $m^3 s^{-1}$ (Box and Ski, 2007; Das and others, 2008).

Conversely, other supraglacial basins have established stream networks that terminate in a moulin, which commonly consists of an initial vertical shaft and subsequent plunge pools (Holmlund, 1988; Gulley, 2009). Moulins are presumed to form from hydrofracturing of water-filled crevasses (Boon and Sharp, 2003; Alley and others, 2005; Van der Veen, 2007; Das and others, 2008) and are believed to persist for multiple years in locations fixed by bedrock geometry (Catania and Neumann, 2010). Unlike crevasse drainage, moulins concentrate the surface meltwater produced over a large area and deliver it to the englacial system at a single point.

Surface crevasses are ubiquitous features of the ablation zone that form when the longitudinal strain rate exceeds the critical fracture toughness of the ice or in response to thermal stress in the spring/early summer (Sanderson, 1978). These features, which are typically linear in nature and transect slopes, prevent large catchment areas from developing, and thus meltwater drainage per crevasse is substantially smaller than for moulins, which typically drain a well-developed catchment basin. Under-appreciated components of the supraglacial hydrologic system are the widespread smaller (5–90 cm) surface and englacial cracks, which we refer to as 'fractures' to differentiate them from typical crevasses. These fractures are observed to persist to depths of 70 m and typically have near-vertical orientations, with surface expressions that are not preferentially aligned with flow direction. Borehole observations in temperate glaciers suggest that surface fractures penetrate to significant depth (~130 m), consisting of near-vertical (~70°) features 0.3–20 cm wide (Fountain and others, 2005). Water flow has been observed to be slow (1–2 cm s^{-1}) in these fractures, but they frequently intersect other fractures, suggesting glaciers may be analogous to 'fractured rock-type aquifers' with high hydraulic conductivity (Fountain and others, 2005; Colgan and others, 2011). Fountain and Walder (1998) suggest that in temperate glaciers the majority of water storage occurs in the englacial, rather than subglacial, hydrologic system. The englacial system likely consists of a combination of well-connected and discrete voids and fractures, which together create a bulk macroporosity of 0.1–10% (Pohjola, 1994; Harper and Humphrey, 1995; Huss and others, 2007). Observations of bubble-free blue-ice bands, both at the surface (exposed as the surface ablates) and at depth with borehole cameras, suggest that meltwater stored in the englacial system frequently refreezes (Pohjola, 1994; Harper and Humphrey, 1995).

2. FIELD SITE

The site of this investigation is a supraglacial catchment basin in the Sermeq Avannarleq ablation zone on the western flank of the GrIS, ~6 km from the ice margin (Fig. 1). Mean surface ablation rate is 1.65 m w.e. a^{-1} (Fausto and others, 2009). The basin is ~360 m below the regional equilibrium-line altitude (ELA). The regional ELA is ~1140 m a.s.l., although inter-annual variations over the past decade range from 1000 to 1400 m a.s.l. (Mernild and others, 2010). The ice in this region is believed to be temperate, based on nearby (<10 km) borehole temperatures (Thomsen and Thorning, 1992). The supraglacial hydrologic network of this basin is arborescent, with multiple tributaries collecting into a single large stream that discharges into a moulin at 69.554° N, 49.899° W and 776 m elevation. Ice thickness at this site is ~530 m. Field observations at our study site in August 2007, 2008 and 2009 indicate that the main trunk stream has maintained an approximate geometry of 1–4 m width and 1–6 m depth, although water has never been observed to fill the entire stream geometry. Panchromatic WorldView-1 satellite imagery (50 cm pixel resolution) of the study site was acquired on 15 July 2009. Manual identification of connecting supraglacial tributaries was used to delineate the extent of the basin. We estimate a basin area, A, of 1.14 ± 0.06 km^2. Comparison of this recent satellite imagery with a historical topographic map (Thomsen, 1986; Thomsen and others, 1988) suggests that since 1985 the supraglacial tributaries have occupied the same general positions and the moulin location has changed by <250 m. From this we speculate that this supraglacial channel network is a recurring annual feature of the local hydrologic system. The moulin is located in the basin bottom (at the lowest elevation), although a series of abandoned moulins exist as a 'string of pearls',

https://doi.org/10.3189/002214311798043735 Published online by Cambridge University Press

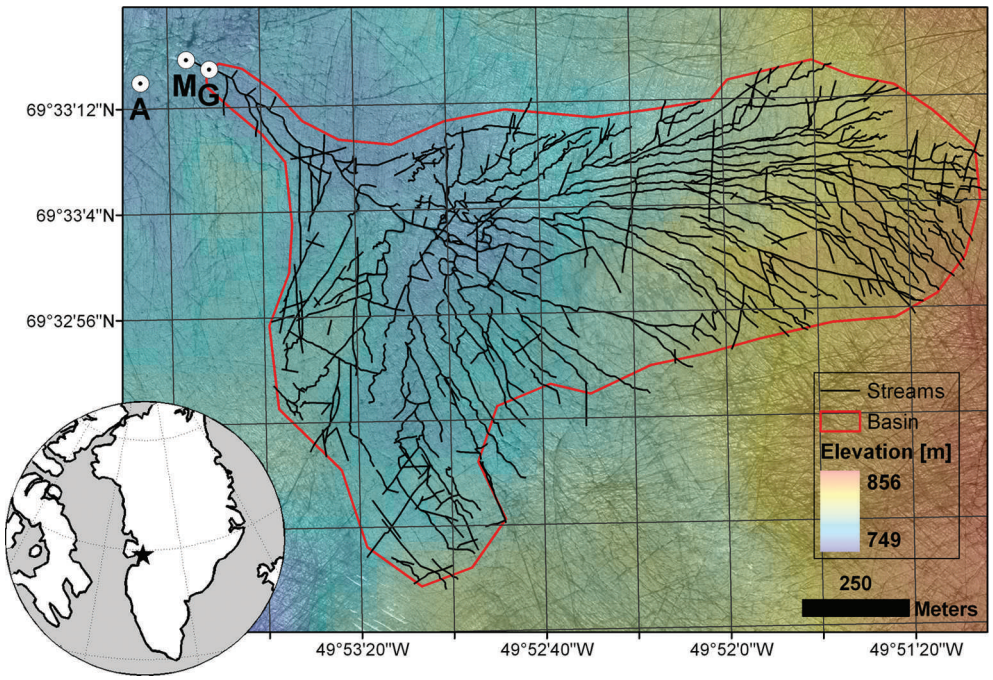

Fig. 1. Supraglacial stream network in West Greenland (inset) overlaid on panchromatic WorldView-1satellite imagery (acquired 15 July 2009) with elevation shading from the Advanced Spaceborne Thermal Emission and Reflection Radiometer (ASTER) global digital elevation model. The locations of the stream gauging station (G), moulin (M) and automatic weather station (A) are identified.

advected towards the ice margin at an annual ice velocity of ~100 m a^{-1}. These abandoned moulins are not regularly spaced and are thus not necessarily annual features. Field observations in 2008 found englacial conduits transporting water into an abandoned moulin shaft at 70 m depth, suggesting while surface entry points may change, the englacial drainage system is relatively persistent (Catania and Neumann, 2010).

Large crevasses (~1 m wide) are observed in the WorldView-1 imagery at the periphery of the basin, but are not present in the basin bottom. Refrozen fractures of bubble-free ice (5–90 cm wide) are observed at the surface across the basin bottom and at depth (~70 m) within a large, abandoned moulin in the basin (Fig. 2a and b), suggesting the widespread existence of refrozen englacial voids and fractures similar to those observed on alpine glaciers (Fountain and others, 2005).

Animation 1. Animation of Extreme Ice Survey time-lapse photographs (every 15 min) of supraglacial stream and gauging station. Full animation available at www.igsoc.org/hyperlink/10J209_animation1.mp4.

3. METHODS

3.1. Data acquisition

A stream gauging station was deployed on the main supraglacial stream ~30 m upstream of the moulin between 3 and 17 August 2009 (day of year (DOY) 215–229; Fig. 2a). It recorded water surface height with a Campbell Scientific SR-50 sonic sensor and stream velocity with a Geopacks MFP51 Flowmeter. The sonic instrument measured instantaneous water surface height at 15 min intervals, while stream velocity was measured as the mean over 15 min intervals. The sonic sensor was installed ~1 m above the water surface, while the flowmeter was installed at the center width of the stream channel at a fixed height. While the absolute position of the impeller was fixed, its relative position fluctuated within the water column as both the stage height varied and the channel incised downwards (Fig. 2a). An automatic weather station (AWS) deployed in 2007 was located ~160 m from the gauging station and measured ice surface height (Campbell Scientific SR-50), air temperature (Vaisala HMP50) and wind speed and direction (RM Young 050103). An Extreme Ice Survey digital camera (Nikon D200, 20 mm lens) was installed ~15 m downstream of the gauging station and recorded photographs every 15 min (Animation 1). These in situ measurements allow us to assess the water budget of this supraglacial stream basin.

3.2. Water mass-balance model

Using conservation of water mass, we may formulate our stream basin-scale water budget as a simple balance of inputs and outputs:

$$0 = (I_{MELT} + I_{RAIN}) - (Q_{MOULIN} + Q_{CREVASSE} + Q_E) + \Delta S, \quad (1)$$

https://doi.org/10.3189/002214311798043735 Published online by Cambridge University Press

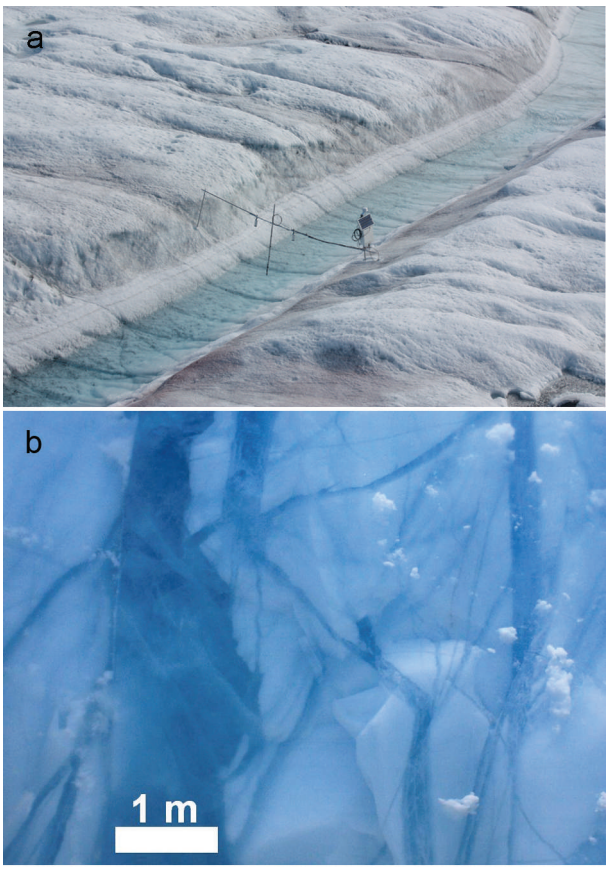

Fig. 2. (a) Oblique aerial photo of the supraglacial stream and gauging station (~30 m upstream from moulin). Note numerous refrozen fractures crossing stream channel. The solar panel is 42 cm × 27 cm and water flow is from right to left in photo. (b) Englacial fractures filled with dark-blue bubble-free refrozen meltwater on the side-wall of a moulin shaft at ~40 m depth.

where I_{MELT} and I_{RAIN} are water inputs to the basin due to ablation and rainfall, Q_{MOULIN}, $Q_{CREVASSE}$ and Q_E are water fluxes from the basin due to moulin discharge, crevasse drainage and evaporation, and ΔS is the rate of change in surface storage. From the absence of supraglacial meltwater ponds within the study area we assume there is no significant change in surface water storage over the study period (i.e. $\Delta S \approx 0$). Field data may be used to constrain all water-budget terms except $Q_{CREVASSE}$, which includes drainage via both crevasses and smaller moulins (<0.25 m diameter) within the basin. We treat this as a free term when solving the water budget, so $Q_{CREVASSE}$ incorporates the uncertainty in all other budget terms. We reformulate the basin-scale water budget as

$$Q_{CREVASSE} = (I_{MELT} + I_{RAIN}) - (Q_{MOULIN} + Q_E). \quad (2)$$

Meltwater production due to ablation was calculated from observed ice surface height change, $\Delta Z_S/\Delta t$, during the study period (Fig. 3). Ice surface height measurements were made every hour. No significant snow or ice deposition occurred during the study period (Animation 1). Surface height change at the AWS location was assumed to be representative of ablation across the basin due to minimal variations in slope, aspect and surface albedo (by August, all snow has melted and the surface is bare ice). Thus, we calculate the hourly meltwater production as

$$I_{MELT} = \left(\frac{\Delta Z_S}{\Delta t}\right) A \frac{\rho_i}{\rho_w}, \quad (3)$$

where ρ_i and ρ_w represent the density of ice (900 kg m^{-3}) and water (1000 kg m^{-3}), respectively. Although the AWS was not equipped to record liquid precipitation, we estimate water input due to rainfall from the in situ Extreme Ice Survey photographic record. The photographic record indicates that only two brief rainfall events occurred over the 15 day study period. The first event, 1.25 ± 0.25 hours in duration, occurred on 3 August 2009 while the second event, 4.25 ± 0.25 hours in duration, occurred on 11 August 2009. Both these rain events fit the description of being 'light' in intensity (<2.5 mm h^{-1}; American Meteorological Society, http://amsglossary.allenpress.com/glossary/search?id=rain1, so we estimate the intensity, R, of the events as 0.5 ± 0.25 and 1.0 ± 0.5 mm h^{-1} respectively. Even assuming extreme intensities (10 mm h^{-1}), the brevity of these events precludes rainfall from being a major term in the cumulative water budget. Combining rainfall intensity and basin area allows the rate of water input due to rainfall to be estimated according to

$$I_{RAIN} = RA. \quad (4)$$

Water output due to moulin discharge was determined from gauge station data, consisting of stage height and water velocity measurements (Fig. 4a and b). Unlike terrestrial river gauging where the bed may be assumed to be constant over short timescales, in supraglacial stream gauging the bed incises into the ice at an appreciable rate. Thus, both the water surface and bed elevations vary relative to the fixed impeller elevation through time. The cross-sectional profile of the supraglacial channel was measured upon installation (day 215). The time-lapse photographic record (Animation 1)

https://doi.org/10.3189/002214311798043735 Published online by Cambridge University Press

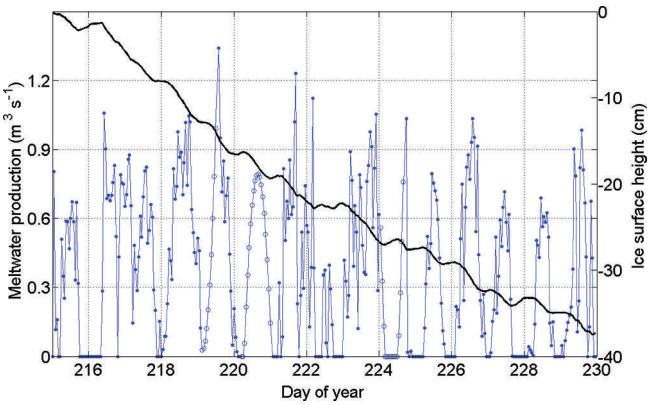

Fig. 3. Observed ice surface height, Z_S (black line), and corresponding instantaneous basin-wide meltwater production from in situ surface height measurements (cf. Equation (3); blue line) over the 15 day study period. Open circles are values interpolated by a high-order polynomial fit during times of instrument error.

and measurements upon gauging-station removal suggest that the assumption of a constant geometry that incised downward is justified. The stream incised into the ice surface at a rate of 3.3 ± 0.47 cm d^{-1}. This was calculated as the slope of a linear best fit through daily minimum stream surface elevation values over the 15 day study period (Fig. 4a). By constraining the stream bed elevation and recording the water surface elevation and cross-sectional profile (Fig. 5a), the cross-sectional area of the stream, A_{CROSS}, can be determined at any time-step via numerical integration.

Depth-averaged velocity values, $\bar{u}$, were multiplied by the cross-sectional stream area (Fig. 4c) to determine moulin discharge:

$$Q_{MOULIN} = \bar{u} A_{CROSS}. \quad (5)$$

However, due to the fixed elevation of the impeller in space and changing water surface height, we develop a site-specific rating curve using velocity values when the impeller was located at 0.37 ± 0.03% of water column height. This is consistent with the assumption that the depth-averaged velocity in turbulent flow occurs at 37% of water column height (Reynolds number $\gg$2000; Anderson and Anderson, 2010). We apply the rating curve ($Q_{MOULIN} = 1.234H^2 - 0.303H$; $n = 88$; $r^2 = 0.99$; Fig. 5b) to calculate moulin discharge at times when the impeller is outside this range of water column heights and after the impeller failed on day 220.

A theoretical rate of water output due to evaporation was calculated based on latent heat flux:

$$Q_E = \frac{\phi_E}{L_S \rho_w}. \quad (6)$$

We assume a latent heat flux, ϕ_E, of 6.8 W m^{-2}, which was

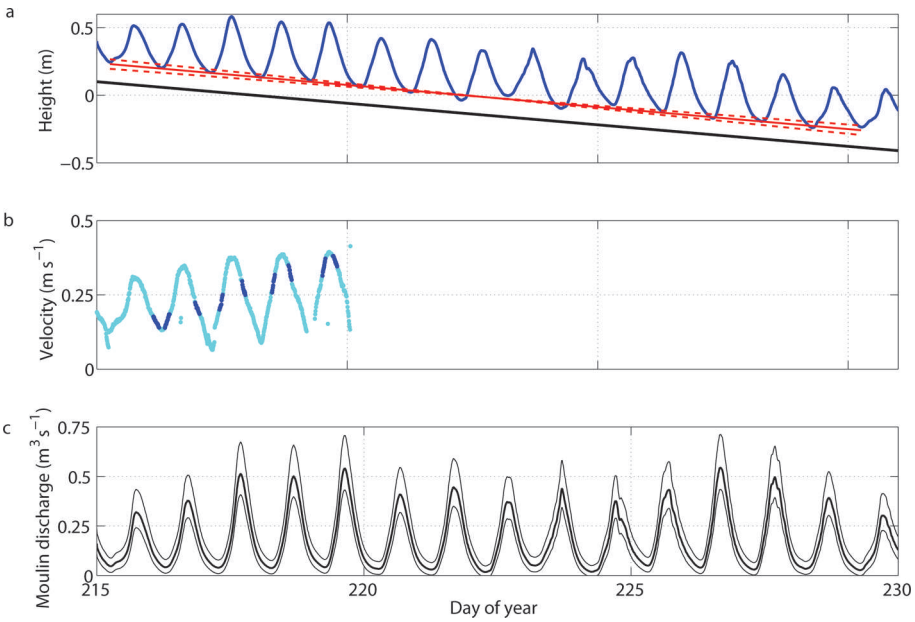

Fig. 4. (a) Water surface height over the 15 day period relative to the impeller elevation (0 m). Black line is stream bottom, which incised at 3.3 ± 0.47 cm d^{-1}. Incision rate is taken as the slope of the minimum stream surface height over the 15 day study period (red lines). (b) Observed stream velocity, u, at all times (cyan) and when located at 0.37 ± 0.03% of the water column height, H, and used to develop the rating curve (blue). Impeller failed on day 220. (c) Calculated instantaneous discharge, Q_{MOULIN} (bold line), $\pm$ error (thin line) of the supraglacial stream as it enters the moulin.

https://doi.org/10.3189/002214311798043735 Published online by Cambridge University Press

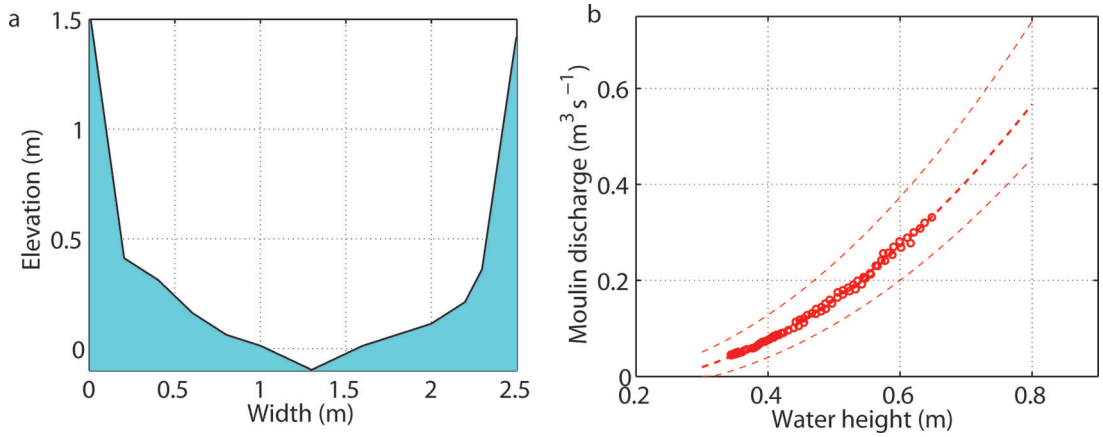

Fig. 5. (a) Cross-sectional area of the supraglacial stream at the gauging station (measured DOY 215). (b) Rating curve ± error used to calculate stream discharge ($Q_{MOULIN} = 1.234H^2 - 0.303H$; $r^2 = 0.99$). Open circles are measured values used to construct rating curve ($n = 88$).

observed in August 2000 at the nearby JAR2 AWS (~17 km south-southwest at 570 m elevation; Box and Steffen, 2001). The latent heat of sublimation, L_S, is taken as 2.834×10^6 J kg^{-1}.

A comprehensive error analysis for each term and the complete water budget is included in the Appendix.

3.3. Crevasse mass-balance model

We developed a simple one-dimensional model to describe the mass balance of both water and ice within an idealized crevasse over multiple melt seasons. This model is meant to serve as a proof of concept that crevasses can significantly dampen the diurnal cycle of meltwater entering the englacial system in comparison to moulins. However, this simplified model is neither meant to close the water budget nor explicitly determine the percentage of refrozen versus discharged meltwater. Further, we do not examine melt-water-driven crevasse hydrofracture (Van der Veen, 2007; Das and others, 2008). Our idealized crevasse has a simple triangular geometry with a depth of 10 m and a width of 0.5 m (Animation 2). The mass of liquid-phase water within a crevasse, M_w, may be described by three terms: (1) the rate at which surface meltwater enters the crevasse, $i\rho_w$, (2) the rate at which water drains from the crevasse, M_w/τ_{res}, and (3) the rate at which liquid water freezes into solid ice within the crevasse, ϕ_q/L_f:

$$\frac{dM_w}{dt} = i\rho_w - \frac{M_w}{\tau_{res}} - \frac{\phi_q}{L_f}, \quad (7)$$

where i is the rate of external meltwater input (m^3 h^{-1}), τ_{res} is the mean residence time of water within the crevasse network (hours), ϕ_q is the heat flux into the ice per unit area (J h^{-1}; Equation (9)) and L_f is the latent heat of fusion (333 550 J kg^{-1}). The rate of external meltwater input can be calculated according to

$$i = a_s d_c dy, \quad (8)$$

where a_s is the modeled surface ablation rate (m w.e. h^{-1}), d_c is the mean crevasse spacing (taken as 25 m; Phillips and others, 2010) and dy is a unit width (1 m). We assume that all meltwater produced on both sides of the crevasse within a distance of $d_c/2$ enters the crevasse. We model daily ablation rate by approximating the annual ablation cycle with a sine function that integrates to the observed annual ablation value at the elevation of the moulin (~1.65 m w.e.; Fausto and others, 2009) over the duration of the melt season (Colgan and others, 2011). Within each day, ablation is distributed over a 12 hour period with a secondary sine function, while the remaining 12 hours of the day experience no ablation. The model is solved at a 1 hour time-step, to resolve diurnal meltwater drainage into the idealized crevasse, using MATLAB's semi-implicit 'stiff' solver (ode15s).

We do not impose a channel or conduit geometry to calculate water discharge from the crevasse to the englacial hydrology system. Instead, we employ a linear reservoir model (cf. Flowers and Clarke, 2002) and simply assign a mean residence time for water within the crevasse network, and thus neglect a possible influence of the englacial drainage system on crevasse discharge. Modeled crevasse pseudo-discharge is therefore equal to the mass of water within the crevasse, M_w, divided by this mean residence

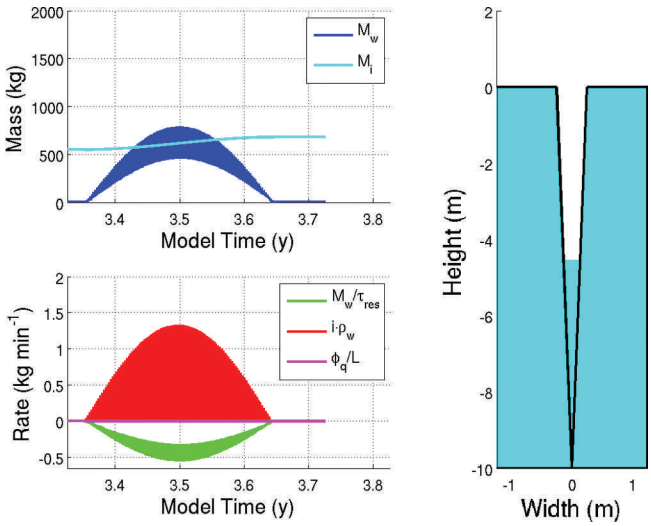

Animation 2. Top: Masses of ice, M_w, and water, M_i, within the idealized crevasse through time. Bottom: Crevasse water mass-balance terms: surface meltwater input, $i\rho_w$, crevasse discharge, M_w/τ_{res}, and refreezing into solid ice, ϕ_q/L. Right: Schematic showing transient refrozen ice (cyan) and water (blue) levels within the crevasse. Full animation available at www.igsoc.org/hyperlink/10J209_animation2.mov.

https://doi.org/10.3189/002214311798043735 Published online by Cambridge University Press

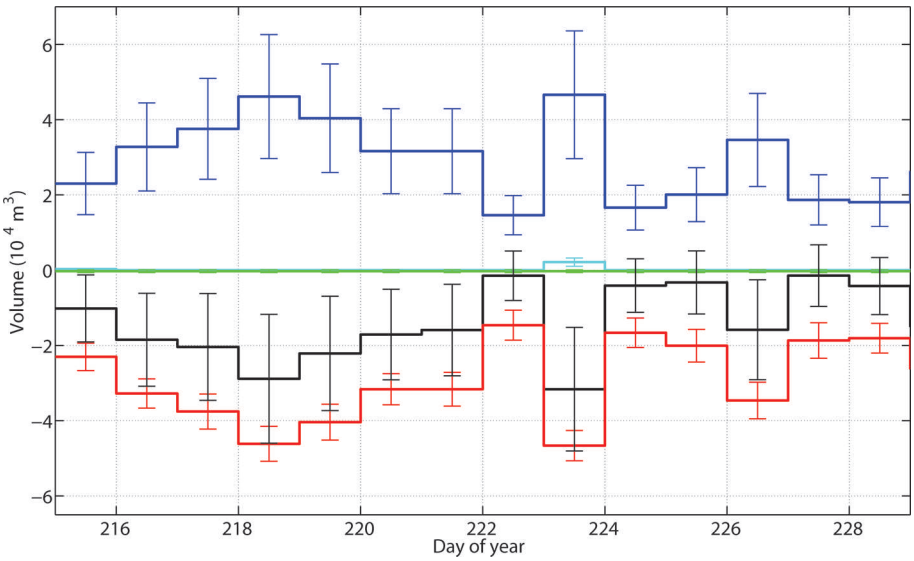

Fig. 6. Time series of daily water budget components for the moulin basin over the 15 day study period. The total input (blue) is the sum of I_{MELT} and I_{RAIN} (cyan) while the total loss (red) is the sum of evaporation (green), $Q_{CREVASSE}$ (black) and Q_{MOULIN}.

time, τ_{res}. To examine the influence of crevasse water residence time in regulating the drainage of supraglacial meltwater, we run the crevasse model with a wide range of mean water residence times (τ_{res} = 1.5, 3, 6, 12, 24, 48 and 96 hours).

Liquid water is also removed from the crevasse through refreezing into solid ice. We calculate heat flux into the ice, ϕ_q, according to

$$\phi_q = kl(T_w - T_i), \quad (9)$$

where k is the conductivity of ice (2.1 W m^{-1} K^{-1}; Paterson, 1994), l is the conduction length (m) of the water/ice interface within the crevasse, and T_w and T_i are the temperature of water within the crevasse and the background temperature of the surrounding ice, respectively (Animation 2). To calculate the transient water/ice interface, l, we assume that water refreezes in the crevasse from the bottom upwards. We also assume the water within the crevasse has a temperature of 0°C, and take T_i as –1.5°C, which is generally consistent with the steady-state summertime temperature in the upper 10 m of the ice column according to an englacial hydrologic model of this region (Phillips and others, 2010). We neglect the heat generated by viscous energy dissipation in the water within the crevasse and hence assume no internal meltwater production. As the mass of water removed from the crevasse by refreezing, M_i, turns out to be negligible in comparison to the modeled crevasse pseudo-discharge, the ϕ_q/L_f term has little influence on the rate at which supraglacial meltwater is transferred to the englacial system.

4. RESULTS

The mean daily rate of surface meltwater production in the basin was $(2.91 \pm 1.04) \times 10^4$ m^3 d^{-1} over the 15 day study period (Fig. 6). In comparison, the mean rate of water input due to rainfall (on days 215 and 223) was 163 ± 83 m^3 d^{-1}. Thus, the total water input due to rainfall over the study period (0.5%) may be considered negligible in comparison to the water input due to surface ablation (99.5%). Water loss due to evaporation was also negligible, responsible for <1%, or 267 ± 374 m^3 d^{-1}, of total water output from the basin. Moulin discharge removed water from the basin at a mean rate of $(1.52 \pm 0.42) \times 10^4$ m^3 d^{-1}. This comprised 52% of water output from the supraglacial basin. Crevasse drainage, the residual of the water budget, comprised 48%, or $(1.40 \pm 1.13) \times 10^4$ m^3 d^{-1}, of water output from the basin. As expected, meltwater production in the basin exhibited a strong radiation-driven diurnal cycle, resulting in meltwater production ranging from 0 to 1.23 m^3 s^{-1}. Peak production occurred at 13:59 local time ± 231 min (15:59 UTC; 12:39 solar time) each day (Fig. 7). Correspondingly, instantaneous moulin discharge, which ranged from 0.017 to 0.54 m^3 s^{-1}, typically reached peak discharge at 16:45 local time ± 24 min (18:45 UTC; 15:25 solar time) each day (Animation 1; Fig. 7). The mean temporal lag between meltwater production and moulin discharge is therefore 2.8 ± 4.2 hours.

We find that the variability of modeled crevasse pseudo-discharge to the englacial system (defined as the difference between daily maximum and minimum over mean crevasse discharge) is nonlinearly dependent on mean water residence time (Fig. 8a). A 'small' increase in mean water residence time produces a disproportionately 'large' dampening of the diurnal meltwater signal. The exponential decay of the modeled crevasse pseudo-discharge variability relative to residence time suggests that crevasses with residence times more than 48 hours significantly dampen meltwater input variability and yield a nearly constant discharge (Fig. 8b; Animation 2).

5. DISCUSSION

The relative distribution of meltwater input into the englacial system via the point source moulin (52%) and distributed crevasse drainage (48%) has important implications for subglacial hydrology and basal sliding. Because crevasses dampen the diurnal cycle of meltwater input to the englacial system, they are more likely to have a quasi-steady-state discharge over short timescales (hours to days). This reduces the likelihood that the englacial and subglacial hydrologic systems will be overwhelmed by surface meltwater input, as

https://doi.org/10.3189/002214311798043735 Published online by Cambridge University Press

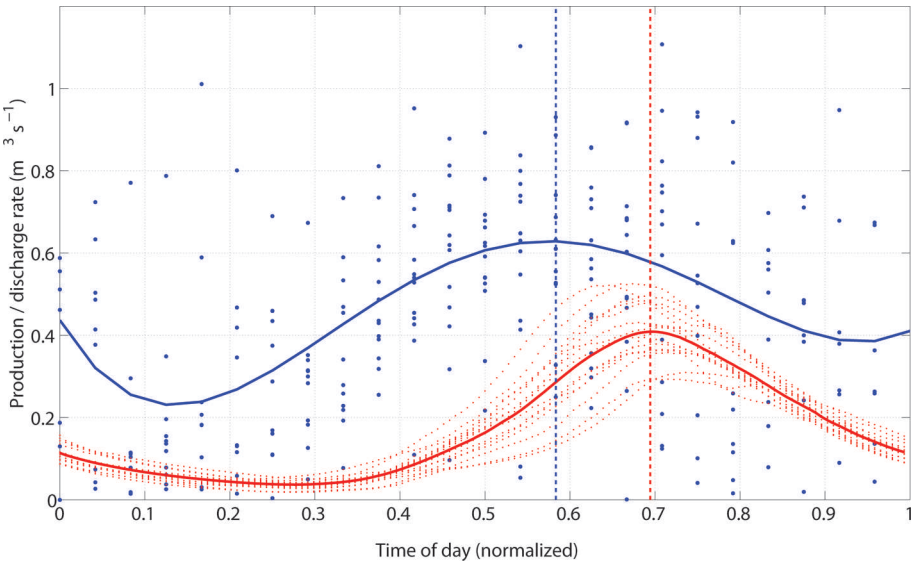

Fig. 7. Daily records of instantaneous meltwater production (blue) and moulin discharge (red) over the study period with mean values (solid colored line). Vertical dashed lines represent timing of peak meltwater production (13:59 local time) and peak moulin discharge (16:45 local time).

they are configured to efficiently drain the meltwater volume. In contrast, moulin discharge has a strong diurnal cycle that varies by more than an order of magnitude and is rapidly transferred from the surface to the englacial system.

Moulin discharge peaks 2.8 ± 4.2 hours after maximum meltwater production. We interpret this as the time necessary for meltwater to flow from across the basin to the entry point at the moulin. To put this observed temporal

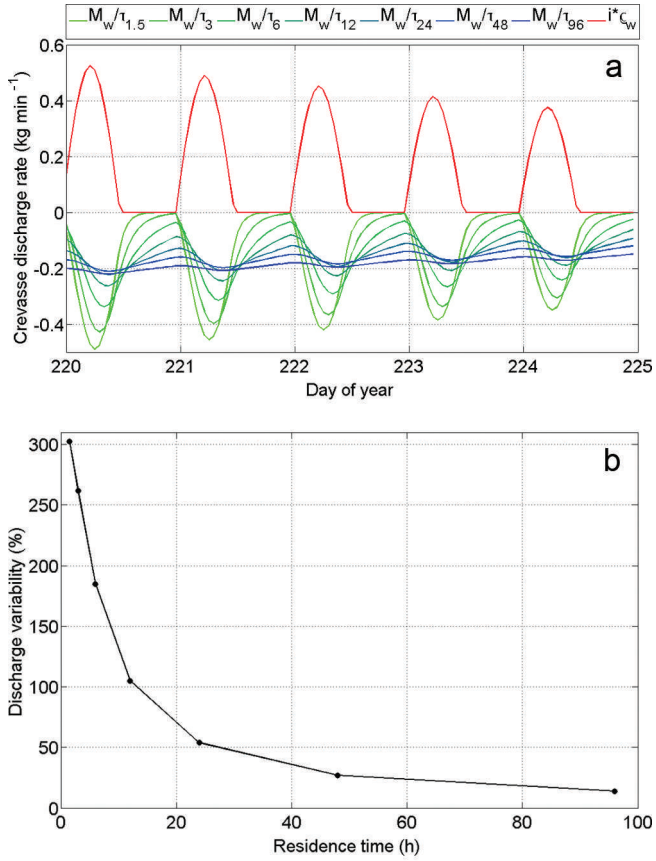

Fig. 8. (a) Crevasse meltwater input, $i\rho_w$ (red), and discharge, M_w/τ_{res}, into the englacial system versus DOY with mean crevasse water residence times, τ_{res}, of 1.5, 3, 6, 12, 24, 48 and 96 hours. (b) Modeled crevasse discharge variability on day 220 (defined as the difference between daily maximum and minimum over mean crevasse discharge) versus mean water residence time.

https://doi.org/10.3189/002214311798043735 Published online by Cambridge University Press

lag into context, we bin the basin area into 100 m increments of increasing distance from the moulin and estimate the travel time for each basin. Assuming an increase in flow velocity as the supraglacial network evolves from percolation (0.05–0.1 m s^{-1}) to tributary channels (0.2 m s^{-1}) to main channel (0.3 m s^{-1}; Fig. 4b), we find an approximate supraglacial travel time for the meltwater to be 2.6 hours, supporting the notion that the observed lag is due to supraglacial transport to the moulin.

Field observations in multiple years using borehole video cameras find that meltwater discharge via the moulin initially freefalls 70–100 m into the ice (Steffen and others, 2009). Previously observed borehole water pressures near our study area (<10 km) were 79–105% of the ice overburden pressure (Thomsen and Olesen, 1991). Modeling also suggests that the englacial water table in the Sermeq Avannarleq ablation zone can exceed 80% of the ice thickness or reside ~100 m below the ice surface at our study site (Colgan and others, 2011). Synthesizing these observations, we speculate that once meltwater reaches a moulin, its transfer to the top of the englacial water table, where the pressure is transmitted to the bed, is nearly instantaneous. Thus, unlike crevasse drainage systems, moulins can propagate the high variability in surface meltwater input to the englacial water table, where these pulses have the capacity to overwhelm subglacial transmission capacity, increasing subglacial water pressure and enhancing basal sliding. This inference supports Shepherd and others (2009), who conclude that the ~2 hour time lag between peak meltwater production and observed vertical uplift and horizontal displacement is primarily the result of supraglacial travel time.

In comparison to moulin discharge, our model suggests that, under reasonable assumptions, crevasses cannot be expected to transfer similar meltwater pulses to the englacial system. By late summer, the daily meltwater input to the crevasse represents only a small portion of the water volume already present therein, so the discharge out of the crevasse is nearly constant with time (Fig. 8a; Animation 2). Recent observations in West Greenland have suggested that englacial hydrologic features, consisting of moulins and englacial channels, persist through the winter (Catania and Neumann, 2010), so maximum residence times of more than half a year may be conceivable. While our range in crevasse mean water residence times, τ_{res}, could be an underestimate, increases in τ_{res} would only act to further dampen the fluctuations in surface meltwater reaching the englacial system. Thus, rather than determining a precise mean water residence time or percentage of meltwater that refreezes in situ, the crevasse mass-balance model theoretically demonstrates that crevasse drainage could substantially differ from moulin discharge in its ability to propagate meltwater pulses to the subglacial hydrologic system.

From our water budget, nearly 50% of surface meltwater produced in the basin is attributed to input into crevasses and small fractures. As this term incorporates the errors of the entire water budget, it contains substantial uncertainty. Nevertheless, it is important to consider the broad implications of this inference. Large crevasses (>1 m wide) are only present at the periphery of the river basin near the topographic divide. Surface ablation rates in this region are high enough to have removed the top ~20 m of ice and crevasses therein by the time the ice has transited from the upstream basin periphery to the basin bottom. Further, crevasses are unlikely to form in the compressive stress environment of the basin bottom. Therefore, it is unlikely that crevasses constitute a large component of the meltwater storage in the study basin. Conversely, observations of refrozen englacial fractures (5–90 cm wide) in our basin, both at the surface and at depths of up to 70 m, suggest that a large volume of meltwater is stored and then refrozen at depth within the ice, releasing latent heat and warming the surrounding ice (Fig. 2a and b). These fractures form in response to ice flow dynamics and temperature gradients (to 5–10 m depth) and likely represent transient features, forming and closing frequently. The role of these englacial fractures in storing meltwater and the timescales on which they operate are unclear, but our observations suggest these features may retain a significant water volume and should be considered in further detail in the future.

The relation between surface meltwater generation and basal sliding has important implications for ice-sheet mass balance. Over the past 30 years, GrIS melt extent, meltwater production and ELA have increased and they are expected to continue to increase over the next century (Abdalati and Steffen, 2001; ACIA, 2004; Box and others, 2006; Hanna and others, 2008). While the combination of higher atmospheric temperatures, increased melt season duration and an expanded ablation zone will result in greater meltwater production, there is substantial uncertainty about the ramifications for supra- and subglacial hydrology and basal sliding velocities. As meltwater production expands to higher elevations of the ice sheet, it is imperative to gain insight into the changing extent and proportion of supraglacial drainage features (i.e. moulins versus crevasses) in order to assess the impact of these drainage types on ice-sheet basal sliding velocity.

6. CONCLUSIONS

A comprehensive water budget is presented for a 1.14 ± 0.06 km^2 supraglacial basin in the Sermeq Avannarleq ablation zone for a 15 day period during August 2009. Meltwater production was the dominant input term to the basin, with an average input rate of $(2.91 \pm 1.04) \times 10^4$ m^3 d^{-1}, of which $(1.52 \pm 0.42) \times 10^4$ m^3 d^{-1}, or 52%, was drained via the moulin in the basin. Crevasse drainage, treated as a free term in the water budget, accounted for 48% of the water output from the basin. Rainfall, evaporation and crevasse refreezing/storage were negligible terms in the August water budget. Meltwater input to the ice sheet via the moulin had a distinct diurnal cycle, peaking at 16:45 local time, 2.8 ± 4.2 hours after peak meltwater production. Combining these in situ observations with previous studies (Thomsen and Olesen, 1991; Shepherd and others, 2009), we suggest that the primary lag in the transfer of meltwater to the englacial water table by moulins is the supraglacial routing of water to the moulin. Once at the moulin, vertical transport to the top of the englacial water table is nearly instantaneous. This rapid transport propagates the variability in surface meltwater production to the englacial water column, possibly overwhelming the drainage capacity and thus causing enhanced basal sliding through increased subglacial water pressure. In contrast, meltwater drainage to the englacial system via crevasses is nearly constant with time, as the diurnal fluctuation in meltwater production is significantly dampened by short-term crevasse storage.

https://doi.org/10.3189/002214311798043735 Published online by Cambridge University Press

ACKNOWLEDGEMENTS

This work was supported by a grant from the NASA Cryospheric Sciences Program. We thank J. Kastengren for assistance in the field and C. Chaapel at Digital Globe for help with acquiring and pre-processing the WorldView-1 image. W.C. was supported by a Natural Sciences and Engineering Research Council of Canada (NSERC) Postgraduate Scholarship and a US National Science Foundation (NSF) Doctoral Dissertation Research Improvement grant. M.A. Werder and an anonymous reviewer provided useful comments that greatly improved the manuscript.

REFERENCES

Abdalati, W. and K. Steffen. 2001. Greenland ice sheet melt extent: 1979–1999. *J. Geophys. Res.,* **106**(D24), 33,983–33,988.

Alley, R.B., T.K. Dupont, B.R. Parizek and S. Anandakrishnan. 2005. Access of surface meltwater to beds of sub-freezing glaciers: preliminary insights. *Ann. Glaciol.,* **40**, 8–14.

Anderson, R.S. and S.P. Anderson. 2010. *Geomorphology: the mechanics and chemistry of landscapes.* Cambridge, etc., Cambridge University Press.

Anderson, R.S. *and 6 others*. 2004. Strong feedbacks between hydrology and sliding of a small alpine glacier. *J. Geophys. Res.,* **109**(F3), F03005. (10.1029/2004JF000120.)

Arctic Climate Impact Assessment (ACIA). 2004. *Impacts of a warming Arctic*. Cambridge, etc., Cambridge University Press.

Bartholomaus, T.C., R.S. Anderson and S.P. Anderson. 2008. Response of glacier basal motion to transient water storage. *Nature Geosci.,* **1**(1), 33–37.

Bartholomew, I., P. Nienow, D. Mair, A. Hubbard, M.A. King and A. Sole. 2010. Seasonal evolution of subglacial drainage and acceleration in a Greenland outlet glacier. *Nature Geosci.,* **3**(6), 408–411.

Boon, S. and M. Sharp. 2003. The role of hydrologically-driven ice fracture in drainage system evolution on an Arctic glacier. *Geophys. Res. Lett.,* **30**(18), 1916. (10.1029/2003GL018034.)

Box, J.E. and K. Ski. 2007. Remote sounding of Greenland supraglacial melt lakes: implications for subglacial hydraulics. *J. Glaciol.,* **53**(181), 257–265.

Box, J.E. and K. Steffen. 2001. Sublimation on the Greenland ice sheet from automated weather station observations. *J. Geophys. Res.,* **106**(D24), 33,965–33,981.

Box, J.E. *and 8 others*. 2006. Greenland ice sheet surface mass balance variability (1988–2004) from calibrated Polar MM5 output. *J. Climate,* **19**(12), 2783–2800.

Catania, G.A. and T.A. Neumann. 2010. Persistent englacial drainage features in the Greenland Ice Sheet. *Geophys. Res. Lett.,* **37**(2), L02501. (10.1029/2009GL041108.)

Catania, G.A., T.A. Neumann and S.F. Price. 2008. Characterizing englacial drainage in the ablation zone of the Greenland ice sheet. *J. Glaciol.,* **54**(187), 567–578.

Colgan, W. *and 7 others*. 2011. The annual glaciohydrology cycle in the ablation zone of the Greenland ice sheet: Part 1. Hydrology model. *J. Glaciol.,* **57**(204), 697–709.

Cutler, P.M. 1998. Modelling the evolution of subglacial tunnels due to varying water input. *J. Glaciol.,* **44**(148), 485–497.

Das, S.B. *and 6 others*. 2008. Fracture propagation to the base of the Greenland Ice Sheet during supraglacial lake drainage. *Science,* **320**(5877), 778–781.

Fausto, R.S., A.P. Ahlstrøm, D. van As, C.E. Bøggild and S.J. Johnsen. 2009. A new present-day temperature parameterization for Greenland. *J. Glaciol.,* **55**(189), 95–105.

Flowers, G.E. and G.K.C. Clarke. 2002. A multicomponent coupled model of glacier hydrology: 1. Theory and synthetic examples. *J. Geophys. Res.,* **107**(B11), 2287. (10.1029/2001JB001122.)

Fountain, A.G. and J.S. Walder. 1998. Water flow through temperate glaciers. *Rev. Geophys.,* **36**(3), 299–328.

Fountain, A.G., R.W. Jacobel, R. Schlichting and P. Jansson. 2005. Fractures as the main pathways of water flow in temperate glaciers. *Nature,* **433**(7026), 618–621.

Gulley, J. 2009. Structural control of englacial conduits in the temperate Matanuska Glacier, Alaska, USA. *J. Glaciol.,* **55**(192), 681–690.

Hanna, E. *and 8 others*. 2008. Increased runoff from melt from the Greenland Ice Sheet: a response to global warming. *J. Climate,* **21**(2), 331–341.

Harper, J.T. and N.F. Humphrey. 1995. Borehole video analysis of a temperate glacier's englacial and subglacial structure: implications for glacier flow models. *Geology,* **23**(10), 901–904.

Hock, R. and R.LeB. Hooke. 1993. Evolution of the internal drainage system in the lower part of the ablation area of Storglaciären, Sweden. *Geol. Soc. Am. Bull.,* **105**(4), 537–546.

Holmlund, P. 1988. Internal geometry and evolution of moulins, Storglaciären, Sweden. *J. Glaciol.,* **34**(117), 242–248.

Howat, I.M., I. Joughin, S. Tulaczyk and S. Gogineni. 2005. Rapid retreat and acceleration of Helheim Glacier, east Greenland. *Geophys. Res. Lett.,* **32**(22), L22502. (10.1029/2005GL024737.)

Huss, M., A. Bauder, M. Werder, M. Funk and R. Hock. 2007. Glacier-dammed lake outburst events of Gornersee, Switzerland. *J. Glaciol.,* **53**(181), 189–200.

Iken, A., H. Röthlisberger, A. Flotron and W. Haeberli. 1983. The uplift of Unteraargletscher at the beginning of the melt season – a consequence of water storage at the bed? *J. Glaciol.,* **29**(101), 28–47.

Joughin, I., S.B. Das, M.A. King, B.E. Smith, I.M. Howat and T. Moon. 2008. Seasonal speedup along the western flank of the Greenland Ice Sheet. *Science,* **320**(5877), 781–783.

Knighton, A.D. 1981. Channel form and flow characteristics of supraglacial streams, Austre Okstindbreen, Norway. *Arct. Alp. Res.,* **13**(3), 295–306.

Marston, R.A. 1983. Supraglacial stream dynamics on the Juneau Icefield. *Ann. Assoc. Am. Geogr.,* **73**(4), 597–608.

Mernild, S.H., G.E. Liston, K. Steffen and P. Chylek. 2010. Meltwater flux and runoff modeling in the ablation area of Jakobshavn Isbræ, West Greenland. *J. Glaciol.,* **56**(195), 20–32.

Nye, J.F. 1953. The flow law of ice from measurements in glacier tunnels, laboratory experiments and the Jungfraufirn borehole experiment. *Proc. R. Soc. London, Ser. A,* **219**(1139), 477–489.

Paterson, W.S.B. 1994. *The physics of glaciers. Third edition.* Oxford, etc., Elsevier.

Perovich, D.K., W.B. Tucker, III and K.A. Ligett. 2002. Aerial observations of the evolution of ice surface conditions during summer. *J. Geophys. Res.,* **107**(C10), 8048. (10.1029/2000JC000449.)

Phillips, T., H. Rajaram and K. Steffen. 2010. Cryo-hydrologic warming: a potential mechanism for rapid thermal response of ice sheets. *Geophys. Res. Lett.,* **37**(20), L20503. (10.1029/2010GL044397.)

Pinchak, A.C. 1972. Diurnal flow variations and thermal erosion in supraglacial melt streams. *In Proceedings of Arctic and Mountain Environments Symposium, 22–23 April, 1972, East Lansing, MI, USA*. East Lansing, MI, Michigan State University.

Pohjola, V.A. 1994. TV-video observations of englacial voids in Storglaciären, Sweden. *J. Glaciol.,* **40**(135), 231–240.

Röthlisberger, H. 1972. Water pressure in intra- and subglacial channels. *J. Glaciol.,* **11**(62), 177–203.

Sanderson, T.J.O. 1978. Thermal stresses near the surface of a glacier. *J. Glaciol.,* **20**(83), 257–283.

Schoof, C. 2010. Ice-sheet acceleration driven by melt supply variability. *Nature,* **468**(7325), 803–806.

Shepherd, A., A. Hubbard, P. Nienow, M. McMillan and I. Joughin. 2009. Greenland ice sheet motion coupled with daily melting in late summer. *Geophys. Res. Lett.,* **36**(1), L01501. (10.1029/2008GL035758.)

Steffen, K., A.E. Behar, D. McGrath, W.T. Colgan, T.P. Phillips and J. Adler. 2009. Monitoring Greenland ice sheet's climate and

exploring moulins. [Abstr. C54A-07.] *Eos,* **90**(52), Fall Meet. Suppl.
Thomas, R., E. Frederick, W. Krabill, S. Manizade and C. Martin. 2009. Recent changes on Greenland outlet glaciers. *J. Glaciol.,* **55**(189), 147–162.
Thomsen, H.H. 1986. Photogrammetric and satellite mapping of the margin of the inland ice, West Greenland. *Ann. Glaciol.,* **8**, 164–167.
Thomsen, H.H. and O.B. Olesen. 1991. Hydraulics and hydrology on the Inland Ice. *Grønl. Geol. Unders. Rapp.* 152, 36–38.
Thomsen, H.H. and L. Thorning. 1992. Ice temperature profiles for western Greenland. *Grønl. Geol. Unders. Rapp.*
Thomsen, H.H., L. Thorning and R.J. Braithwaite. 1988. Glacier-hydrological conditions on the Inland Ice north-east of Jacobshavn/Ilulissat, West Greenland. *Grønl. Geol. Unders. Rapp.* 138.
Van de Wal, R.S.W. *and 6 others*. 2008. Large and rapid melt-induced velocity changes in the ablation zone of the Greenland Ice Sheet. *Science,* **321**(5885), 111–113.
Van den Broeke, M. *and 8 others*. 2009. Partitioning recent Greenland mass loss. *Science,* **326**(5955), 984–986.
Van der Veen, C.J. 2007. Fracture propagation as means of rapidly transferring surface meltwater to the base of glaciers. *Geophys. Res. Lett.,* **34**(1), L01501. (10.1029/2006GL028385.)
Willis, I.C., K.S. Richards and M.J. Sharp. 1996. Links between proglacial stream suspended sediment dynamics, glacier hydrology and glacier motion at Midtdalsbreen, Norway. *Hydrol. Process.,* **10**(4), 629–648.
Zwally, H.J., W. Abdalati, T. Herring, K. Larson, J. Saba and K. Steffen. 2002. Surface melt-induced acceleration of Greenland ice-sheet flow. *Science,* **297**(5579), 218–222.

APPENDIX

Error analysis

Here we assess the uncertainty in each term of the water budget. We assume that the uncertainties in each term used to calculate a water-budget term are independent and randomly distributed through time. Therefore, we may use a quadratic fractional sum to estimate the fractional uncertainty in each term of the water budget, which is multiplied by the term to yield absolute uncertainty. We estimate uncertainty in basin area, $\sigma[A]$, as ±5% (or 0.06 km^2), based on repeated manual delineations.

Absolute uncertainty in the rate of meltwater production, $\sigma[I_{\mathrm{MELT}}]$, is a function of the uncertainty in surface height measurements, the spatial variability in surface height changes within the basin and the surface area. First, the uncertainty of the surface height measurement is

$$\sigma[Z_{\mathrm{S}}] = \sqrt{(\sigma[Z_{\mathrm{S1}}])^2 + (\sigma[Z_{\mathrm{S2}}])^2}, \quad \text{(A1)}$$

where instrument uncertainty, $\sigma[Z_{\mathrm{S}}]$, is ±1 cm and the $_{\mathrm{S1}}$ and $_{\mathrm{S2}}$ subscripts represent the surface elevation measurements at the two times over which the change is calculated. We assumed the spatial variability in surface ablation is negligible because elevation and aspect vary only slightly across the small basin. Thus, the uncertainty in meltwater production (Equation (3)) is

$$\sigma[I_{\mathrm{MELT}}] = \sqrt{\left(\frac{\sigma[Z_{\mathrm{S}}]}{Z_{\mathrm{S}}}\right)^2 + \left(\frac{\sigma[A]}{A}\right)^2} \cdot I_{\mathrm{MELT}}. \quad \text{(A2)}$$

Uncertainty in the rate of water input due to rainfall (Equation (4)), $\sigma[I_{\mathrm{RAIN}}]$, is the sum of three terms:

$$\sigma[I_{\mathrm{RAIN}}] = \sqrt{\left(\frac{\sigma[R]}{R}\right)^2 + \left(\frac{\sigma[t]}{t}\right)^2 + \left(\frac{\sigma[A]}{A}\right)^2} \cdot I_{\mathrm{RAIN}}, \quad \text{(A3)}$$

where the uncertainty in rainfall intensity, $\sigma[R]$, is estimated as ±0.25 and ±0.5 mm h^{-1} for rain events 1 and 2 respectively, and uncertainty in the duration of each rain event, $\sigma[t]$, is taken as ±15 min (the sampling interval of the Extreme Ice Survey camera). t represents the duration of the rain event.

Uncertainty in the rate of water output due to moulin discharge (Equation (5)), $\sigma[Q_{\mathrm{MOULIN}}]$, is the sum of two terms:

$$\sigma[Q_{\mathrm{MOULIN}}] = \sqrt{\left(\frac{\sigma[\bar{u}]}{\bar{u}}\right)^2 + \left(\frac{\sigma[A_{\mathrm{CROSS}}]}{A_{\mathrm{CROSS}}}\right)^2} \cdot Q_{\mathrm{MOULIN}}, \quad \text{(A4)}$$

where uncertainty in depth-averaged velocity, $\sigma[\bar{u}]$, is taken as one-half of the difference between the depth-averaged velocities calculated assuming impeller height differences of ±10 cm, and $\bar{u}$ represents the mean depth-averaged velocity over the rating period. The uncertainty range in the channel cross-sectional area, $\sigma[_{\mathrm{ACROSS}}]$, is calculated at each time-step by using a ±10 cm uncertainty in the elevation of the channel bed. We assume that the error which the Q_{MOULIN} rating curve introduces is negligible, given the high regression coefficient of the relation ($r^2 = 0.99$). We speculate that this good fit is due to the relatively simple geometry of the channel cross section.

Uncertainty in the rate of water output due to evaporation (Equation (6)), $\sigma[Q_{\mathrm{E}}]$, only originates from uncertainty in the latent heat flux, $\sigma[\phi_{\mathrm{E}}]$, which we take as 9.3 W m^{-2}, the observed August standard deviation in latent heat flux at nearby JAR2 AWS (~17 km south-southwest at 570 m elevation; Box and Steffen, 2001).

$$\sigma Q_{\mathrm{E}} = \frac{\sigma[\phi_{\mathrm{E}}]}{\phi_{\mathrm{E}}} Q_{\mathrm{E}} \quad \text{(A5)}$$

Assuming that the uncertainties in each term of the water budget are independent and randomly distributed through time, absolute uncertainty in the rate of water output due to crevasse discharge, $\sigma[Q_{\mathrm{CREVASSE}}]$, can be estimated as the quadratic sum of the fractional uncertainty in each term of the water budget times the value of Q_{CREVASSE}:

$$\sigma[Q_{\mathrm{CREVASSE}}] = \sqrt{(\sigma[I_{\mathrm{MELT}}])^2 + (\sigma[I_{\mathrm{RAIN}}])^2 + (\sigma[Q_{\mathrm{MOULIN}}])^2 + (\sigma[Q_{\mathrm{E}}])^2}. \quad \text{(A6)}$$

MS received 14 November 2010 and accepted in revised form 29 July 2011